University of
St Andrews

LRRC15: a Regulator of Immune Function in the Tumour Microenvironment

Submitted as a 2025 Summer Research Project as part of the
Laidlaw Scholars Programme

Laidlaw Scholar:
Grace Stephens-Spada
Supervised by
Prof. David Harrison

LRRC15: a Regulator of Immune Function in the Tumour Microenvironment

G. Stephens-Spada, I.H. Um, J. Woon, D. Harrison

Null Hypothesis: There is no correlations between LRRC15 expression and the occurrence of three specific types of innate immune cells (myeloid-derived suppressor cells, M2 macrophages and M1 macrophages).

Introduction

Leucine-rich repeat containing 15 protein (LRRC15) is a cell-surface protein coded for by a gene of varying length found on the third of the 23 chromosome pairs which make up the human genome (National Library of Medicine, 2025). It consists primarily of 15 consecutive leucine amino acid molecules which form what is predominantly an extracellular protein (Ray U et al., 2022) found on a few specific cell types. This expression pattern supports the idea that LRRC15 is an extracellular receptor which plays a role in cell-to-cell adhesion, receptor-ligand binding and target recognition (Krishnamurty A.T at el., 2022). However, despite this knowledge, the precise role of LRRC15 still remains unknown. In order to further investigate the location and function of LRRC15, tissue samples can be exposed to specifically-designed antibodies which often have fluorophores – a type of molecule which emits visible light after UV stimulation – bound to their Fc region to enable visualisation of LRRC15 within the tissue (Thermo Fisher Scientific, 2025). This method is known as immunofluorescence. Alternatively, they can have a signal molecule such as horseradish peroxidase which, when exposed to other chemical compounds, produces a visible colour by causing precipitation of a coloured product from a colourless precursor. This method is known as immunohistochemistry (See Figure 1).

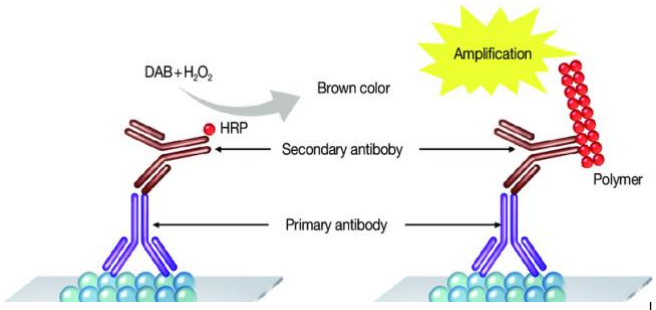

Figure 1.
The left of the diagram explains the process of using immunohistochemistry to label and visualise specific antigens within tissues. The right of the diagram displays the process of using immunofluorescence to label and visualise specific antigens within tissues.
(Kim et al., 2016)

LRRC15 is sparsely expressed in healthy tissue, appearing almost exclusively in innate immune barriers such as the cardia and pylorus sections of the stomach, tonsils, spleen, osteoblasts and hair follicles (Purcell J.W et al., 2018) This is an indication as to LRRC15's involvement in innate immune function. Furthermore, mutations in these extracellular receptors have been seen to occur in individuals with autoimmune diseases such as Crohn's disease, multiple sclerosis and rheumatoid arthritis (Ray U et al., 2022) However, LRRC15's expression is dysregulated in cancers; it has been observed to be upregulated on the surface of cancer cells themselves and is greatly upregulated on cancer associated fibroblasts (CAFs) (Ray U et al., 2022). CAF's role includes producing collagen fibres which form part of the stroma – the extracellular substance which serves as scaffolding in between the sections of tissue which are formed primarily of cancer cells (Belhabib I et al., 2021). This selective expression makes LRRC15 a very suitable target for immunotherapy as it would result in fewer of the unwanted side effects that are caused by binding and activating of therapeutic drugs in areas of the body other than the tumour.

The tumour microenvironment (TME) can be separated into components of cancer cells and other components of stroma, the latter comprising of fibrous extracellular matrix proteins, such as collagen, elastin, and polysaccharides, such as glycosaminoglycans (Frantz C et al., 2010). It contains a variety of different cell types including fibroblasts, cancer associated fibroblasts (CAFs), mesenchymal stem cells, adipocytes and various immune cells (Ray U et al., 2022). While this extracellular matrix is involved in the structural integrity of the TME, particular cells in the stroma also influence the development of the cells around them and thus are responsible for their proliferation, migration, appearance and function (Alberts B et al., 2002). The structure of each TME is specific to different types of tumours, and this is in part why different cancers react in different ways to the same treatments. For example, tumours characterised by being particularly vascularised would be best treated with a drug which limits the development of new blood vessels such as angiogenesis inhibitors (National Cancer Institute, 2018), while those with a greater proportion of stroma would likely be best inhibited using treatments which specifically target proteins and receptors found more exclusively in stroma, potentially like LRRC15.
Once activated, CAFs encourage tumorigenesis, which is achieved through immunomodulation (this is the changing availability of different types of immune cells within the tumour, often leading to it having a localised immunosuppressed state), through angiogenesis (the growth of new blood vessels which supply the tumour with the required nutrients it needs to progress), and metabolic remodelling (this involves a shift from aerobic to anaerobic metabolism), all of which encourage proliferation of the tumour and resistance to therapy.
LRRC15 is also expressed on the apical surface of trophoblast cells (Ray U et al., 2022) – these are cells found on the surface of the placenta which help it implant into the uterine wall by infiltrating its surface. This further exemplifies LRRC15's likely role in cell-to-cell adhesion and supports the theory that LRRC15 may be involved in the invasive nature of certain solid tumours.

This presence of LRRC15 in placental tissue becomes even more interesting when we consider the localised immunosuppression found in pregnancy; while the mother is not themselves immunosuppressed, there must be an element of immunosuppression within the uterus to prevent the maternal immune system from attacking the developing foetus whose paternal DNA is foreign to the mother. This is achieved by the placenta, which is another immune barrier. Furthermore, fibroblasts are found in areas of wound healing, producing collagen for the formation of scar tissue to prevent bleeding and cytokines for the recruitment of immune cells to prevent infection (Ciadai F et al., 2022).

The development of immunotherapy has brought into scrutiny the immunology of the tumour microenvironment. The presence of different immune cells varies throughout the stages of cancer, with exclusion of pro-inflammatory immune cells and invasion of anti-inflammatory immune cells being more characteristic of later stage cancers with worse prognoses – this results in the reduced effectiveness of immunotherapy against these later stage cancers. As noted above, LRRC15 is implicated in having roles in several different immunologically related scenarios and since it is thought to also be upregulated within the TME of certain cancers, it has gained recent attention as a possible localised immune regulator and therefore a possible target for immunotherapy. The three innate immune cells which have been theorised within this study to respond to the level of LRRC15 in the TME, including M1 macrophages, M2 macrophages and myeloid-derived suppressor cells (MDSCs). M1 and M2 macrophages are at opposite ends of an inflammatory scale, with M1 macrophages expressing primarily CD86 surface cell markers and being the most pro-inflammatory and phagocytic and M2 macrophages expressing primarily CD206 surface cell markers and being the most anti-inflammatory and pro-fibrous repair. However, macrophages can often be found at a number of different positions along this scale and their phenotype can shift along the scale depending on environmental conditions which are often determined by

CAFs in the stroma – this shift in phenotype is called polarization (Strizova Z et al., 2023). Moreover, MDSCs are immunosuppressive cells which supress the function of several cytotoxic immune cells such as CD8+ T cells (Zhai Y et al., 2024) and natural killer cells (Bruno A et al., 2019). LRRC15 is theorised to aid in the decreased occurrence of pro-inflammatory immune cells such as M1 macrophages which are thought to impede tumorigenesis, while it decreases the expression of anti-inflammatory immune cells which are thought to contribute to tumorigenesis (Luo F et al., 2025). This means that developing a drug which could inhibit LRRC15 would allow the re-entry of pro-inflammatory immune cells into the TME in order to destroy the cancer cells without causing excessive adverse effects.

The purpose of this study is to investigate to what extent LRRC15 controls the immunological status of the TME by controlling the presence of different innate immune cells within the TME, and thereby how LRRC15 may influence the metastasis of tumours, which it has been noted to do (Ray U et al., 2022). Understanding how LRRC15's role in controlling immunotherapy affects prognosis would help us understand which types of cancers would be most susceptible to treatment by immunotherapy and at which stage of their development. Although we set out to use ovarian cancer samples, we were not able to access the necessary clinical data attached to the samples to be able to complete our analysis, therefore we have instead used melanoma tissue samples.

Methodology

1) Multiplex Immunofluorescence

Three 4 micrometre-thick sections were cut from a tissue microarray (TMA) formalin-fixed paraffin-embedded (FFPE) recipient block - which was created using 44 melanoma tumour sample cores of melanoma tumour tissue with a diameter of 0.6mm - and dried onto glass slides at 65 °C in an oven. Between the three sections this gave a total of 132 cores. These slides were dewaxed at 72°C for 30 seconds in dewax solution (Leica biosystems, AR9222) and then rehydrated using absolute alcohol and 0.5% Tris-buffered saline with Tween 20 (TBST) buffer. Antigens within the tissue cores often become masked during fixation into the FFPE blocks, so antigen retrieval must be performed for 20 minutes at 100°C using Epitope Retrieval solution 1 (ER1) buffer (Leica biosystems, AR9961) to re-expose these antigens so that they can later be bound to by antibodies and identified (Biotechne et al, 2019). 3% Peroxide block (Sigma, H1009) was used for 8 minutes to quench the endogenous peroxidase enzyme naturally present in the tissue to prevent false background staining (Biognost, 2023), followed by Serum-free protein block (Sigma-Aldrich, B6429) for 10 minutes in order to further avoid non-specific background staining.

Rabbit-raised LRRC15 primary antibody (Abcam, ab150376, 1:1500), was then incubated on the slide for 40 minutes; these antibodies bind to LRRC15 proteins in the tissue samples. An anti-rabbit secondary antibody reagent (polymer), conjugated with the horseradish peroxidase enzyme (HRP) was incubated on the slide for 30 minutes. Tyramide signal amplification (TSA) using Cy5 fluorophore-conjugated tyramide (Akoya Biosciences, NEL745001KT), was used for 7 minutes to visualise LRRC15 (See Fig.1).

Heat-induced stripping was undertaken at 95 °C using ER1 buffer in order to remove redundant antibodies and to avoid cross-reactions with second primary antibodies and with secondary antibodies.

A Leica Bond RX Autostainer (Leica Biosystems) was used to perform automated multiplex immunofluorescence to enable sequential cycles of the technique described, first using CD86 primary antibody (CST 91882, 1:400) with Cy3 fluorophore-conjugated tyramide (Akoya Biosciences, NEL744001KT) to enable visualisation and finally using CD11b primary antibody (Abcam, ab52478, 1:1500) with FITC-fluorophore conjugated tyramide (Akoya Biosciences, NEL741001KT) to enable visualisation.

The multiplex immunofluorescence (mIF) cycle was concluded with Hoechst (H3570) counterstaining for 15 minutes. The slides were then mounted using Prolong gold

antifade reagent (Life Technologies Corporation, Invitrogen P36930).

2) Image Acquisition of fluorescence images
Scanning using a fluorescence profile with Zeiss Axio Scan Z1 Digital Slide Scanner (Catalog #000000-2085-000) was done with acquisition at 2x2 binning at 20 magnification. For LRRC15, CD86 , CD11b, and Hoechst a fluorescence profile was used to produce four fluorescence images which were then superimposed to make a single fluorescence multiplex image with four channels.

3) Immunohistochemistry
Upon completion of mIF scanning, the sections were un-coverslipped in TBST buffer and heat-induced stripping of bound antibodies was performed using ER1 buffer. Rabbit-raised CD206 primary antibody (abcam, ab64693, 1:12000) was incubated on the sides for 30 min. An anti-rabbit-polymer (Leica Biosystems, DS9800) conjugated with horseradish peroxidase (HRP) was then incubated for 15 minutes. 3, 3'-diaminobenzidine (DAB) (Leica Biosystems, DS9800 kit) was incubated for 5 minutes.
Heat induced stripping was performed again, followed by S100 primary antibody (Leica Biosystems, PA0031, 1:12000) incubation, visualised by Green chromogen. Haematoxylin counterstain was undertaken and the sections were mounted with Prolong gold anti-fade reagent.

4) Image acquisition of brightfield images
A brightfield profile was used with a Zeiss Axio Scan Z1 Digital Slide Scanner (Catalog #000000-2085-000) to scan CD206 (brown) and S100 (green) under 10 magnification to produce two brightfield images.

5) Image Analysis
Halo AI ™ image analysis platforms (v 4.0.5107.488) (Halo AI) were used to carry out images analysis on the scanned multiplex images. The brightfield images were deconvoluted to convert CD206 and S100 channels into pseudo-fluorescence channels (See Figure 2). The deconvolved images were registered with their respective multiplex immunofluorescence image, allowing the two to be mapped on to each other and thereby superimposed precisely to avoid blurring in the final fused image (See Figure 3). These images are then fused to produce one AI-generated image with six channels including DAPI, CD11b, CD86, LRRD15, CD206 and S100 (DAPI refers to Hoechst (H3570), the stain used to identify all nuclei by staining DNA) (See Figure 4). After image fusion, the TMA cores are segmented so that the computer was able to recognise each core within each tumour microarray image as separate, so that the cores could be individually analysed.
To carry out the analysis, a Random Forest-Tissue vs Background (RF-Tissue VS BG) classifier was made. Random Forest is a model which utilises between 500 – 1000 decision trees to enable a computer to predict future outcomes based on data it has encountered before (Donges N, 2021). A classifier is an algorithm which the Halo AI can use to analyse what is contained within a digital image. These algorithms were created by highlighting samples of different tissue types or cells so that the AI programme might be able to "learn" what in

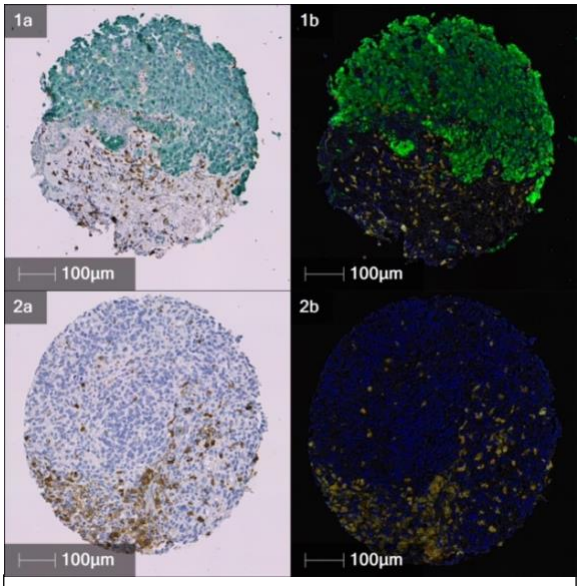

Figure 2.
- 1a and 2a: two brightfield images.
- 1b and 2b: the same two images once deconvolved; they now contain two pseudo-fluorescence channels of CD206 (green) and S100 (orange).

[Images by author]

the image refers to different cells or types of tissue. This particular classifier allowed Halo AI to distinguish tumour tissue from the glass background of the slide (See Figure 5). Once all the cores had been analysed with this classifier, they were quality controlled. To achieve this all the cores were checked and any areas of the images which were deemed to show false staining, such as necrotic regions, areas of folded tissue or the outer border of the cores where any surplus antibody can soak back into the tissue, were manually edited out – all these examples, if not removed before final batch processing, can make it seem that target receptors are expressed more strongly in these areas than they really are. Two new classifiers – RF-Tumour VS NO-Tumour and RF-LRRC15 VS NO-LRRC15 - were then created to distinguish between sections of S100-positive sections and S100-negative sections, and to identify the location of the LRRC15 protein within the tissue cores, respectively (See Figure 6). These were used to enable Halo AI to calculate the proportion and relative location of the targeted innate immune cells in relation to LRRC15.

In order to create analysis algorithms which could phenotype CD11b, CD86 and CD206 positive cells, individual nuclei were first identified by Halo AI Default Nuclear segmentation classifier (v 4.0.5107.488) using the DAPI channel. Then membrane segmentation was undertaken using a Halo AI default membrane segmentation classifier (v 4.0.5107.488) for three different channels – CD11b, CD86 and CD206. Batch processing was then undertaken by Halo AI to quantify the expression of CD206, CD86 and CD11b, corresponding to the expression of M2 macrophages, M1 macrophages and myeloid-derived suppressor cells, respectively, within the tissue samples.

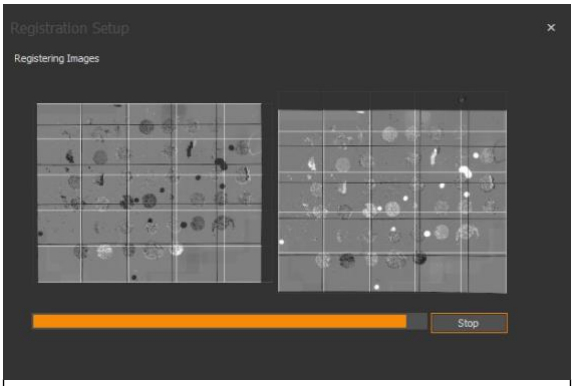

Figure 3.
Registering of an immunofluorescence image and it's respective deconvolved brightfield image so that they can map precisely on to each other and then be fused.
[Image by author]

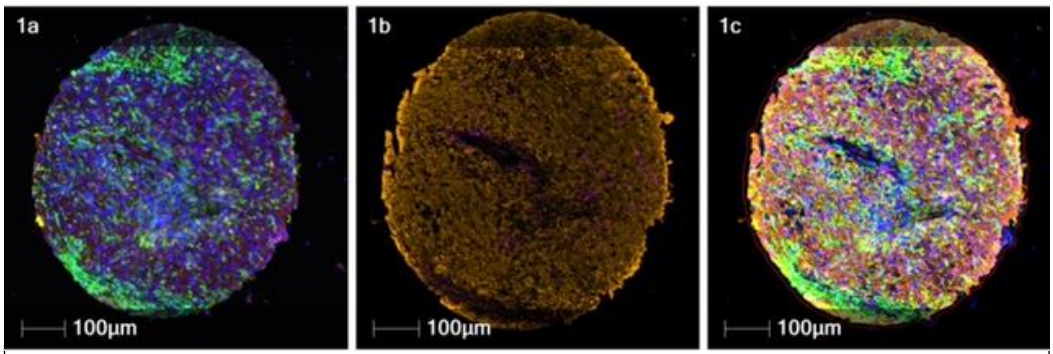

Figure 4.
- 1a: a multiplex immunofluorescence image with four channels: CD11b, CD86, LRRC15 and DAPI
- 1b: a deconvolved brightfield image with two pseudo-fluorescent channels: CD206 and S100
- 1c: the two images, both of which were images of the same tissue core, fused to make one image containing six channels.

[Images by author]

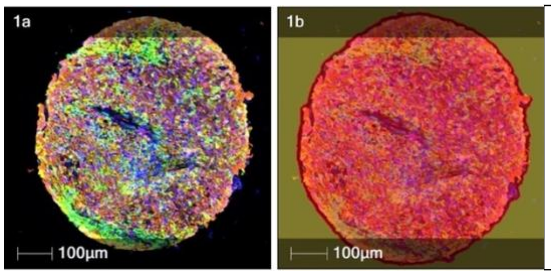

Figure 5.
Random Forrest-Tissue vs Background classifier being used to distinguish between sections of the image pertaining to tissue and those pertaining to background.
[Images by author]

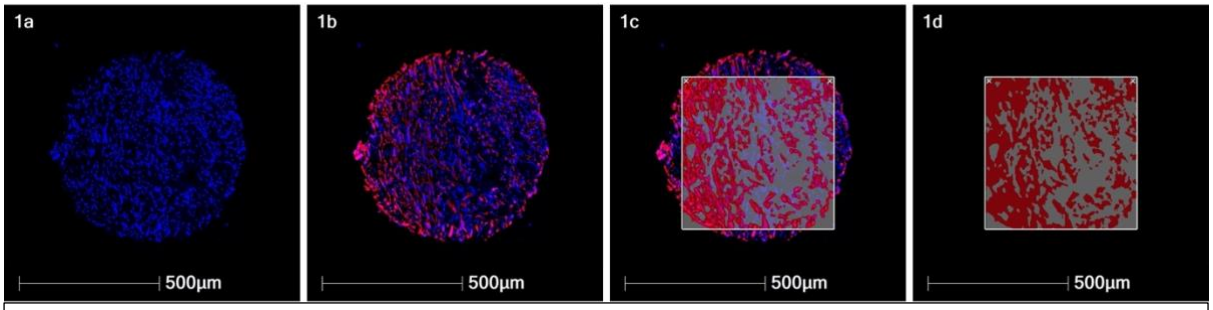

Figure 6.
- 1a: an image of a tissue core displaying only the DAPI channel
- 1b: an image of the same tissue core displaying both DAPI and LRRC15 channels
- 1c and 1d: real-time tuning being used to allow observation of the areas which the AI platform has identified as being LRRC15 positive. The real-time tuning function can be used while creating a classifier to ascertain the accuracy of the AI's "understanding" of what is LRRC15 positive.

[Images by author]

Average densities were calculated for each immune cell in Excel, along with LRRC15 histoscores using the expression levels collected by Halo AI.
Two-tailed Mann Whitney tests was completed in Excel and thus p-values were calculated to ascertain the statistical significance of the difference between the density of each of the three immune cells and of LRRC15 expression within non-metastatic samples versus metastatic samples. Correlation coefficients were calculated to quantify the existence or absence of any correlations between the expression of each immune cell and the presence of LRRC15 within the tissue cores. Two-tailed T tests were carried out to ascertain the statistical significance of the potential correlations observed.

Results

While these results display several observations which were and several which were not predicted when the study was initiated, none were statistically significant. Note that S100 is a surface receptor primarily found on melanoma cells; it has been used in this study to distinguish patterns of expression within areas of TME made up of tumour cells or those made up of surrounding stroma.

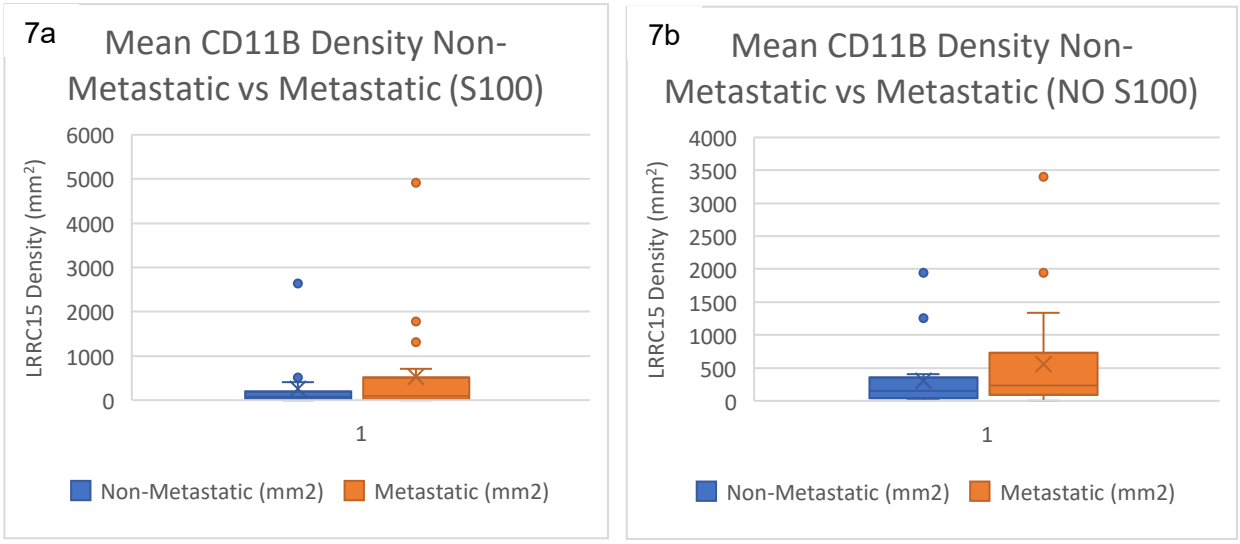

Figure 7.
7a and 7b: These graphs show that the average CD11b density is higher in metastatic S100-positive and S100-negative tissue than in non-metastatic. However, there is considerable overlap between the box plots in each graph. Furthermore, their respective p-values are 0.36812 and 0.41222 for S100-positive and S100-negative data, respectively; both these values show that the difference within both graphs is not statistically significant.

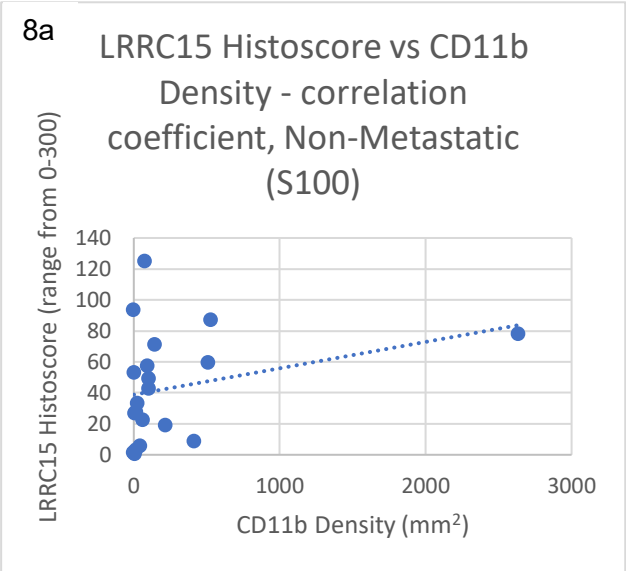

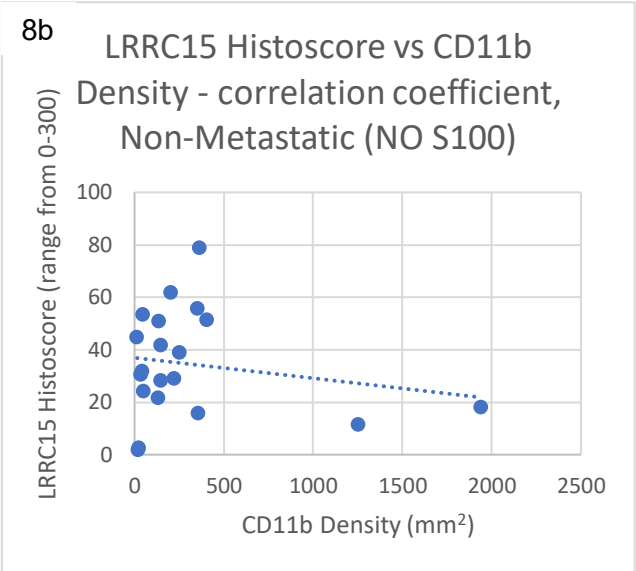

Figure 8.
8a: This displays a positive trend between the density of CD11b-positive cells and the presence of LRRC15 among cancer cells in non-metastatic tumour samples, with a correlation coefficient of +0.286063 (6.s.f) and a p-value of 0.915832; this p-value suggests that there is no statistically significant correlation.

8b: This displays a negative trend between the density of CD11b-positive cells and the presence of LRRC15 within the stroma in non-metastatic tumour samples, with a correlation coefficient of -0.180947 (6.s.f) and a p-value of 0.458489; this p-value suggests that there is no statistically significant correlation.

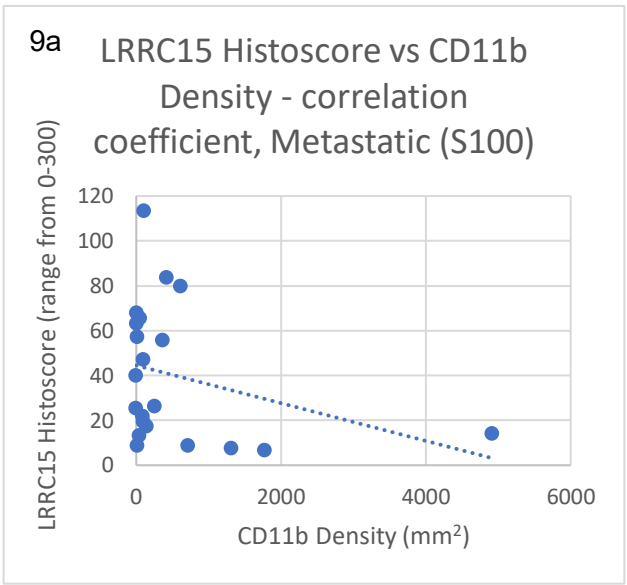

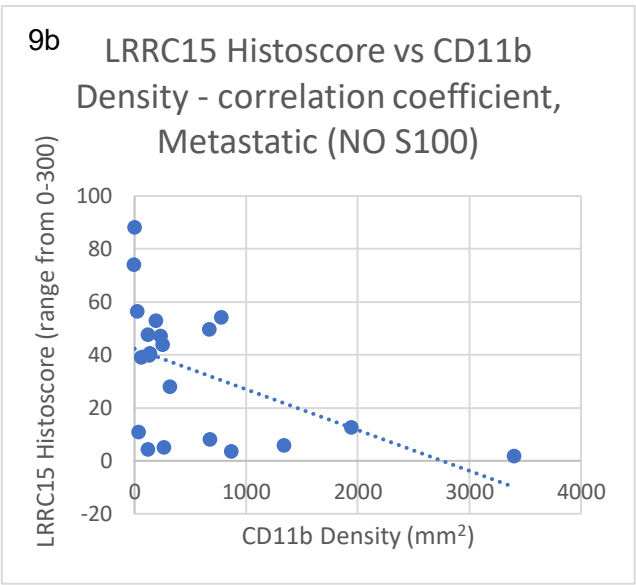

Figure 9.
9a and 9b: These display negative trends between the density of CD11b-positive cells and the presence of LRRC15 among cancer cells and within stroma in metastatic tumour samples. The correlation coefficient within S100-positive tissue is -0.305826 with a p-value of 0.189752. The correlation coefficient within S100-negative tissue is -0.498138 with a p-value of 0.025398. These p-values suggest that there is no statistically significant correlation

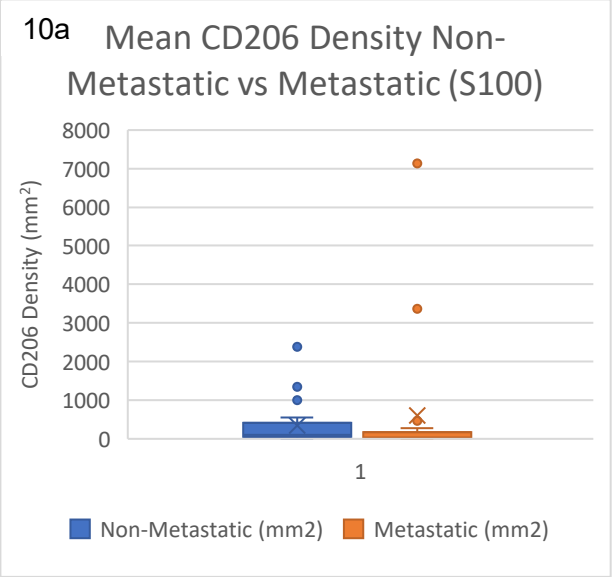

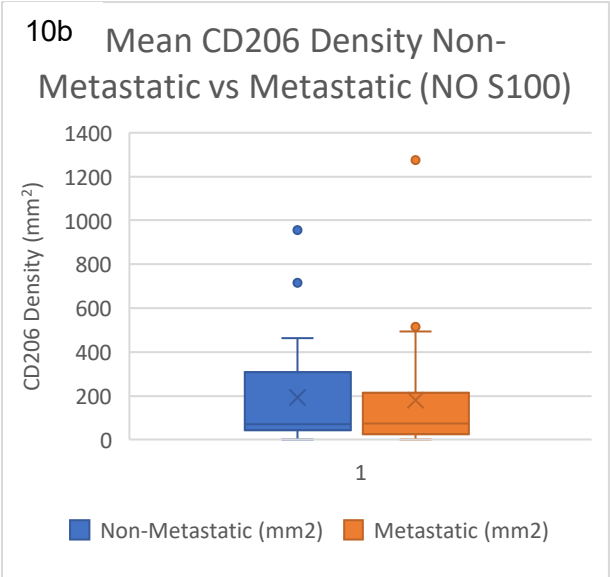

Figure 10.
10a and 10b: Both these graphs show that there was a higher average of CD206-positive cells present in both the S100-positive and the S100-negative metastatic tumour samples than in the non-metastatic samples. However, both box plots in both graphs visibly overlap. Furthermore, the p-values for S100-positive and S100-negative tissues are 0.09296 and 0.72786, respectively; both these values show that the difference within both graphs is not statistically significant.

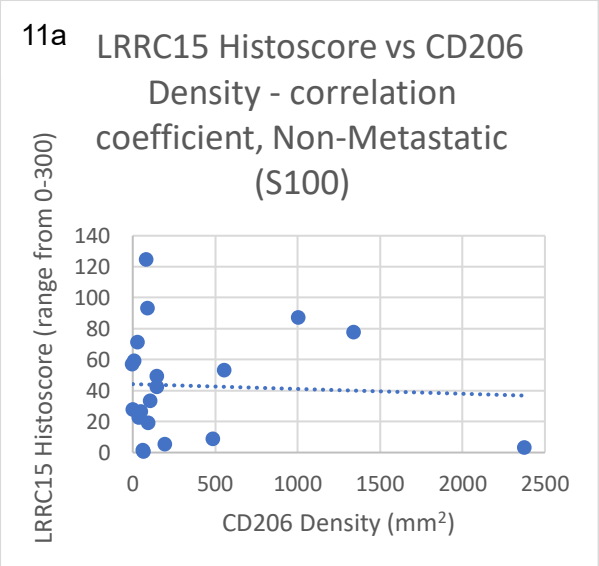

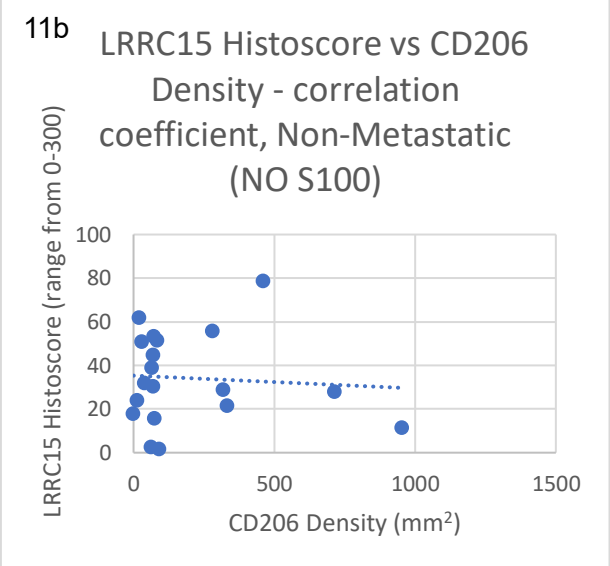

Figure 11.
11a and 11b: These display negative trends between the density of CD206-positive cells and LRRC15 expression within both S100-positive and S100-negative regions of non-metastatic tumour samples. The correlation coefficient within S100-positive tissue is -0.053317 with a p-value of 0.828380. The correlation coefficient within S100-negative tissue is -0.082531 with a p-value of 0.736951. These p-values suggest that there is no statistically significant correlation.

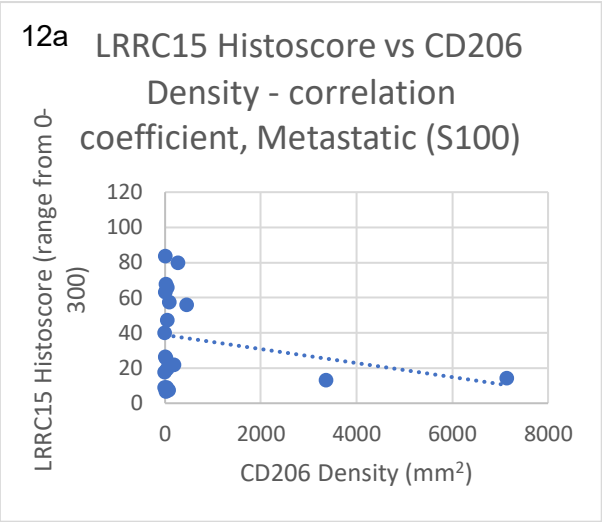

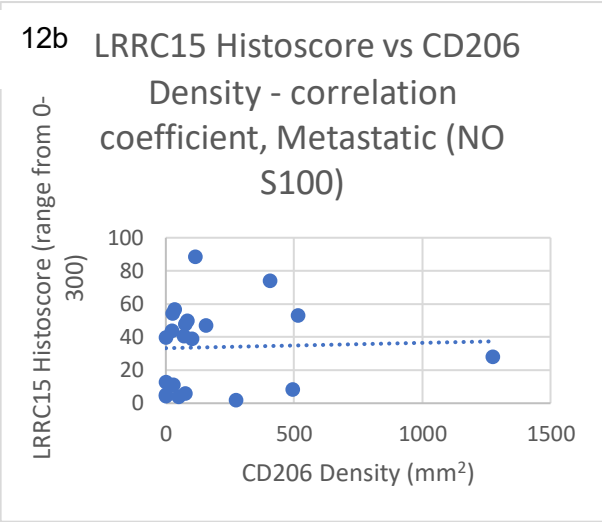

Figure 12.
12a: This displays a negative trend between the density of CD206-positive cells and LRRC15 expression in S100-positive regions of non-metastatic tumour samples with a correlation coefficient of -0.261021 and a p-value of 0.280420. This p-value suggests that there is no statistically significant correlation.

12b displays a positive trend between the density of CD206-positive cells and LRRC15 expression in S100-negative regions of non-metastatic tumour samples with a correlation coefficient of +0.037804 and a p-value of 0.874272. This p-value suggests that there is no statistically significant correlation.

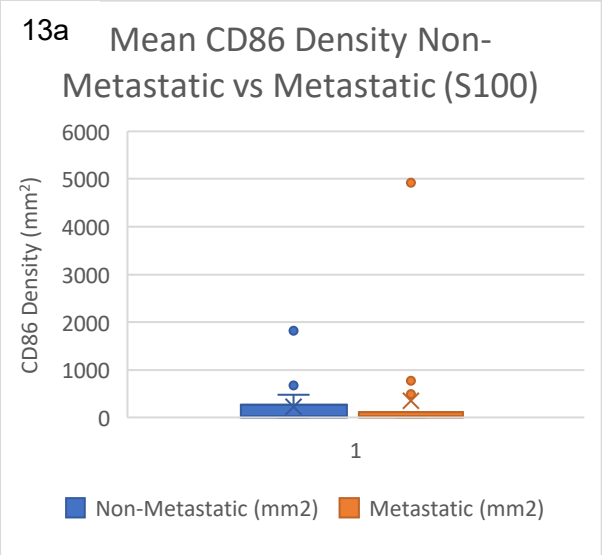

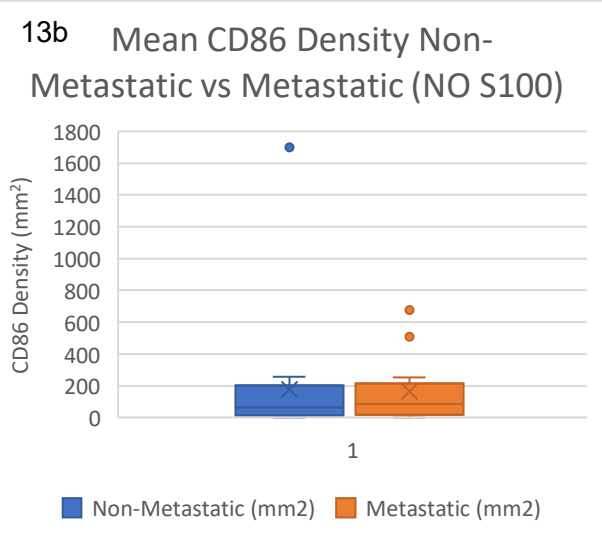

Figure 13.
Although there was a higher average of CD86-positive cells present in both the S100-positive and the S100-negative metastatic tumour samples than there was in the non-metastatic samples, there is evidently overlap between the box plots in both graphs. Furthermore, the p-values are 0.84148 and 0.94420 for S100-positive and S100-negative tissues, respectively, both of which show that the difference between non-metastasic and metastatic samples in both graphs is not statistically significant.

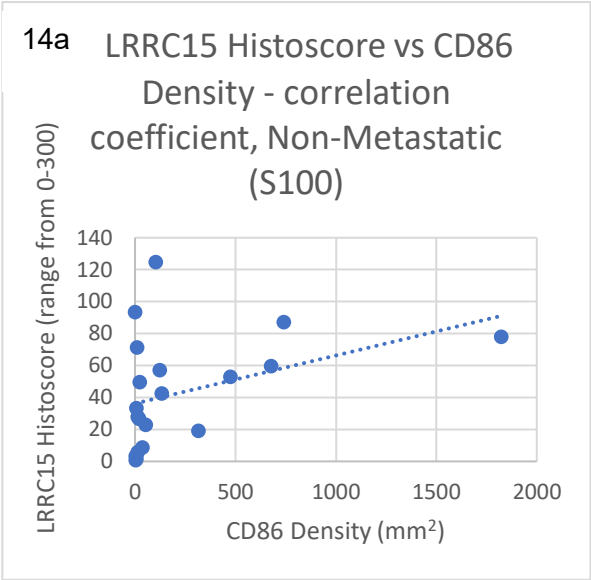

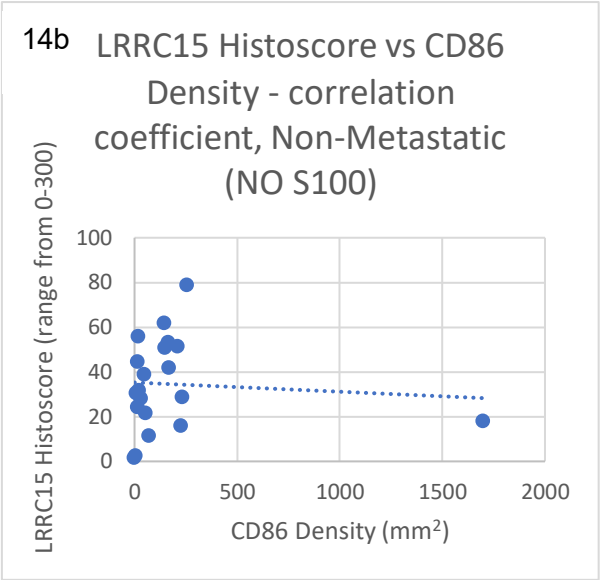

Figure 14.
14a: This displays a positive trend between the density of CD86-positive cells and LRRC15 expression in S100-positive regions of non-metastatic tumour samples with a correlation coefficient of +0.378702 and a p-value of 0.109849. This p-value suggests that there is no statistically significant correlation.

14b: This displays a negative trend between the density of CD86-positive cells and LRRC15 expression in S100-negative regions of non-metastatic tumour samples with a correlation coefficient of -0.074438 and a p-value of 0.761996. This p-value suggests there is no statistically significant correlation.

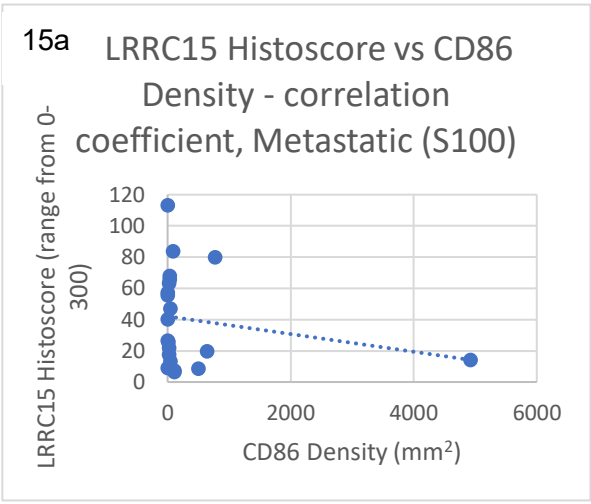

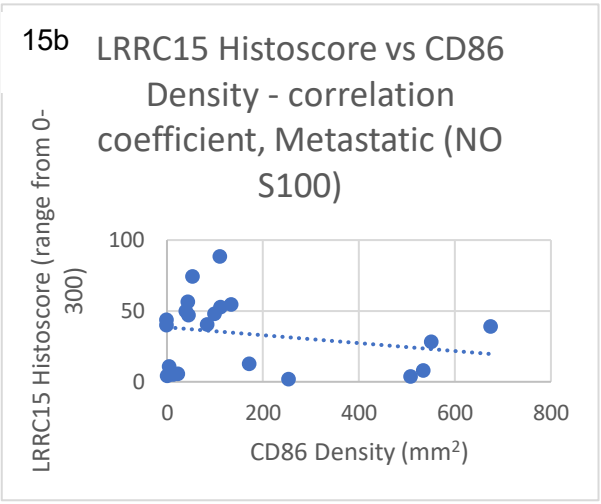

Figure 15.
15a and 15b: These display a negative trend between the density of CD86-positive cells and LRRC15 expression within both S100-positive and S100-negative regions of non-metastatic tumour samples. Within S100-positive tissue the correlation coefficient is -0.198946 with a p-value of 0.400415. The correlation coefficient within S100-negative tissue is -0.233834 with a p-value of 0.321076. Both these p-values suggest that there are no statistically significant correlations.

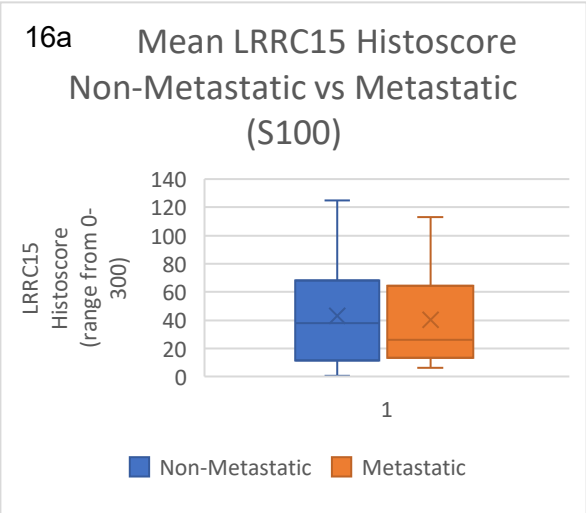

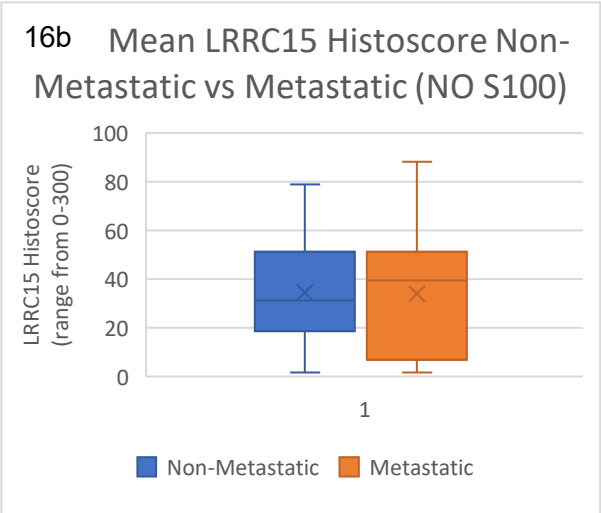

Figure 16.
This shows that there was a greater density of LRRC15 present on S100-positive non-metastatic cells than on S100-positive. However, there is evidently considerable overlap between the non-metastatic and metastatic sample sets within each graph. Furthermore, the p-values for the S100-positive and S100-negative samples are 0.88866 and 0.86502, respectively; these show that there is no statistically significant difference between non-metastatic and metastatic samples in S100-positive or S100-negative tissue.

Discussion

The numbers of myeloid-derived suppressor cells (MDSCs), M1 macrophages and M2 macrophages and the expression of LRRC15 within tissue samples of melanoma were measured using the HALO AI ™ image analysis platforms (v 4.0.5107.488) and from these the average cellular density in the TME was calculated for each immune cell. From the expression levels of LRRC15 a histoscore was calculated using Excel, allowing both the quantity and location of LRRC15 expression to be taken into account. Using the densities of these immune cells and the LRRC15 histoscores, correlation coefficients were calculated to analyse the role of LRRC15 in controlling the presence of the three aforementioned innate immune cells and T Tests were done to assess the significance of any correlations.
Although some trends were seen, there were no meaningful correlations between the cellular density of any of the innate immune cells and the presence of LRRC15. In light of this, it is important to assess the methods used in this study to explore whether they or how they were executed could explain the absence of hypothesised correlations. In this study there were three main points within the methodology which must be considered. These were (i) the creation of the Random Forrest Tissue vs Background classifier, (ii) the quality controlling of the tissue cores and (iii) the creation of a LRRC15 vs NO LRRC15 classifier. These all involve human expertise and have within them subjective judgements, which of course leaves room for human error.
Furthermore, when creating classifiers, multiple examples of each tissue type were provided to ensure that the AI platform was able to accurately identify these same tissues in the future using this classifier – in practicality this creates a running mean, where the longer the mean runs (that is, the more examples provided for the AI platform), the more precise it is likely to be. However, the mean's accuracy is still dependent on the examples provided for the AI platform by the human operating it. To avoid as much human error as possible, it was made sure that expertise was gained from other more experienced members of the team who were more well practiced in interpreting tissue samples using the Halo AI ™ image analysis platforms (v 4.0.5107.488). However, it is plausible that not all human error was removed and if considerable error was

made this would have noticeably impacted the results. For example, if an area of necrosis in one of the tissue cores was missed during quality control and not removed before batch processing, then the density of all immune cells would have been measured to be much higher than they were in reality, thus skewing the results. Furthermore, since none of the antigens used to identify any of the innate immune cells observed in this study are expressed solely on these immune cells, false staining can occur and be measured, where these antigens are bound to while expressed on cells other than the specific innate immune cell they were used to identify in this study and which they are primarily expressed on. This is considerably difficult to pick up on when, as in the case of this research, only one antigen is being targeted to identify each immune cell. Moreover, due to it being such a small sample size, if this were to happen with even one core it would cause a significant change to the results. Another less avoidable outcome of the quality control process is that every time an area perceived to contain false staining is edited out of the digital images then a small amount of usable tissue is lost, thereby shrinking the already small sample size even further and making it harder to produce representative results.

The use of artificial intelligence in modern medicine is fast increasing (Basu k et al., 2020). The form of machine deep learning used in this study has only recently become readily available as a tool used for researching digital images of tissues and yet it has the potential to change essential elements of diagnostic oncology. In this study, it was used to more efficiently and accurately calculate the expression of different cell markers within tumour samples, and while even this added efficiency is hugely helpful in assisting researchers in their role of “manually” analyzing patient biopsies, the role of AI need not end here. Using past patient data, platforms such as HALO AI could be used to generate algorithms using biomarkers - such as the potential biomarker LRRC15 - within digitalized images to predict the stage, likelihood of metastasis and prognosis of a tumour, all within a matter of moments. Using this method, it would also be possible to predict the effectiveness of different immunotherapies by either calculating the number of pro-inflammatory immune cells in the TME directly from digitalized images of tumour samples, or by creating an algorithm which utilizes past data to quantify the relationship between the level of LRRC15 expression and the level of immune cell invasion into the TME to accurately estimate the availability of immune cells within the tumour. This analysis would further develop the extent to which doctors can deliver medical treatment personalized to each patient, increasing treatment effectivity and decreasing the need for toxic and non-discriminatory chemotherapies.
What must be noted however is the risk of unidentified human error. Once algorithms are made, it may become easy to rely solely on them and because these algorithms are only as good as the skills and expertise of the person who created them, they should be used with this in mind to avoid missed diagnoses.

Despite there being no significant correlations, there were differences which, while unable to imply a correlation themselves, are interesting and worthy of further research. One example is the level of LRRC15 in S100-positive and S100-negative cells when observed in both non-metastatic versus metastatic states. While in S100-postive tissue – therefore among cancer cells - less LRRC15 was observed in metastatic tumour samples than in non-metastatic samples, in S100-negative tissue – therefore stroma – this trend was reversed, and more LRRC15 was recorded in metastatic samples in comparison to non-metastatic samples. Assuming momentarily that this trend might also be seen in a bigger cohort, it would suggest that LRRC15 has potential as a biomarker for cancer prognosis, where an increased stromal LRRC15 expression is indicative of a more progressed disease and therefore a worse prognosis. To explore more about how this pattern of expression reflects how LRRC15 would stimulate tumour development, we have to consider LRRC15’s role on CAFs. It has been mentioned that CAF’s make up a large proportion of the stroma within the TME and contribute to its structure and characteristics by producing angiogenic

factors, growth factors, chemokines and cytokines (Kwa M.Q et al., 2019). LRRC15's expression on CAFs can be induced by TGF-β (Storey C.M et al., 2024), a signaling molecule which, as well as encouraging other tumorigenic features such as avoiding apoptosis, promoting cell proliferation and silencing pro-inflammatory immune cells (Chan M.K et al., 2023), promotes the upregulation of vascular endothelial growth factor (VEGF) which stimulates the development of more blood vessels. This supplies the cancer with more substances such as glucose so it can continue metabolizing in the absence of oxygen (Fang L et al., 2020). It is possible that the reason that more LRRC15 is observed in the stroma compared to among cancer cells is because the cancer cells are less exposed to TGF-β, which is produced by CAFs in the stroma. This highlights the potential for LRRC15 to be used both as a marker of prognosis which identifies areas of increased TGF-β production, but also as a therapeutic target to be utilized by potential therapies which aim to limit the production of TGF-β and hence limit the tumorigenic features that TGF-β promotes. However, it must be stressed that this cannot be confirmed by the results of this study owing to the lack of statistically significant differences between the metastatic and non-metastatic sample sets in both S100-positive and S100-negative tissue. It therefore remains speculation which requires confirmation by further research.

The average level of MDSCs, M1 macrophages and M2 macrophages in both S100-positive and S100-negative tissues were seen to be slightly higher in metastatic samples compared to in non-metastatic samples, raising the possibility that all three innate immune cells may have tumorigenic capabilities. While this cannot be confirmed using this data due to its lack in statistical significance, it is interesting to consider the potential roles of these immune cells in facilitating the development of cancer. MDSCs have been seen to reduce the pro-inflammatory capabilities of CD8+ T cells and Natural Killer cells (Joshi S et al., 2022), lowering the body's natural defense against the growing tumour. M2 macrophages are anti-inflammatory and promote angiogenesis and TME remodeling (Cendrowicz E et al., 2021), encouraging tumour growth. M1 macrophages, are pro-inflammatory and generally thought to encourage an immune response within the TME and therefore reduce cancer development (Liu J et al, 2021) – this is interesting considering the fact they were also observed more commonly in metastatic samples rather than non-metastatic samples, but as these results aren't conclusive we cannot draw any conclusions from this and more extensive research is needed to ascertain whether M1 macrophages can truly encourage tumour development. Even just considering their known roles, all three seem to have the potential to be targets of immunotherapies against cancer to some extent. It would therefore be interesting to understand more about how the roles of these immune cells determine how they impact the development of cancer and whether, when observed in larger sample sizes or in the context of other cancer types, there are any significant correlations between their expression and LRRC15 expression. If correlations were to be found in the future, this would likely encourage further research into how LRRC15 would achieve this function; the significance of this being that it would encourage the development of immunotherapies which target LRRC15 in a method similar to that of checkpoint inhibitors – checkpoints are molecules present on certain immune cells which allow them to identify your cells as "self" and they usually serve to deactivate pro-inflammatory immune cells so that your immune system doesn't destroy your own cells (Benelli R et al., 2023). However, cancer cells often also express these checkpoints, and therefore they remain undetected and undestroyed by the immune system (Taefehshokr N et al., 2020). Checkpoint inhibitors prevent this binding between cancer cells and immune cells. Assuming that there were correlations between LRRC15 expression and the density of immune cells within the TME, this inhibition might result in an increased effectiveness of immune cells to impede the development of the tumour.

It has been mentioned that one of the locations where LRRC15 is found in healthy tissue is on trophoblasts cells, at the periphery of the placenta as it implants into the uterine wall. It would therefore be interesting to find out more about the immediate cellular environment within and around trophoblast cells at the end of the first trimester once the placenta is fully implanted; if LRRC15 is even in part responsible for the invasive nature of trophoblast cells, then it seems necessary to consider which factors prevent the trophoblast cells from invading further than the uterine wall, like they might do in an invasive cancer. Once understood, this knowledge might provide further opportunities for the development of LRRC15-inhibiting cancer therapies in the future, assuming that a link between LRRC15 expression and increased invasive cellular behavior is confirmed.

From our results, we are unable to confirm or refute the role of LRRC15 in regulating the innate immune system and thus it has no potential to be utilised as a biomarker to predict cancer prognosis. Further research is needed to ascertain whether this is because LRRC15 truly plays no meaningful role in orchestrating the immune system and is not reliably over-expressed in metastatic cancers or whether it is because our sample size was simply too small to provide results which displayed these functions. If the latter, then the likelihood of LRRC15 being a biomarker is very low. It is also possible that LRRC15 plays a role in regulating the immunological environment of types of cancer other than melanoma or that it orchestrates other immune cell types. A further area of exploration is that LRRC15 on its own is not a biomarker, but in combination with other phenotypic features may indicate that particular molecular pathways are active in some cases and not others.

Conclusion

Although a range of both expected and unexpected trends have been observed within the results of this study, none of them have statistically significance and therefore we cannot be reliably assured that there should be a link between LRRC15 expression and the density of MDSCs, M2 macrophages and M1 macrophages. Solely based on this research, we cannot reject the null hypothesis due to the results of our statistical tests, but this study may indicate that with more extensive research and access to bigger data-sets, there may be potential for the discovery of patterns of expression to come to light in the future. Further research is needed to more completely comprehend the true extent and causation of these trends so that the function of LRRC15 in regulating the innate immune system can be properly understood.

Acknowledgments

I would like to thank Lord Laidlaw for very generously providing me the funds to carry out this research via The Laidlaw Scholars Foundation, without which I would not have been able to embark on this project.

I would also like to thank my supervisor, Prof. David Harrison, and his research team, namely In Hwa Um and Jessie Woon, for their unrelenting assistance throughout this research. I would also like to thank Prof. Derralyn Hughes, for her help and advice during my application to the Laidlaw Scholars Programme.

Finally, I would like to thank my family, my fellow St Andrews Laidlaw Scholars and Theo A.M. Amies for their constant support.

References

1.
Biognost (Zagreb, Croatia). Peroxide Block [Internet]. 2023 [cited 2025 Aug 31]. Available from: https://www.biognost.com/product/peroxide-block/
2.
Bio-Techne, R&D Systems. Antigen retrieval methods [Internet]. Minneapolis (MN): R&D Systems; 2019 [cited 2025 Aug 31]. Available from: https://www.rndsystems.com/resources/protocols/antigen-retrieval-methods
3.

Sigma Aldrich. Blue-White Screening & Protocols for Colony Selection. Merck [Internet]. 2025;1(1). Available from: https://www.sigmaaldrich.com/MX/en/technical-documents/technical-article/genomics/cloning-and-expression/blue-white-screening
4.
Knöfler M, Pollheimer J. IFPA Award in Placentology Lecture: Molecular regulation of human trophoblast invasion. Placenta. 2012 Feb;33(33):S55–62.
5.
Dong SW. The role of LRRC15-SCG5 in ECM protein binding as a prognostic signature for urothelial carcinoma. American Journal of Cancer Research [Internet]. 2025 [cited 2025 Aug 31];15(5):2301–18. Available from: https://pmc.ncbi.nlm.nih.gov/articles/PMC12163458/
6.
Ray U, Jung D, Jin L, Xiao Y, Dasari S, Sayantani Sarkar Bhattacharya, et al. Targeting LRRC15 Inhibits Metastatic Dissemination of Ovarian Cancer. Cancer Research [Internet]. 2022 Mar 15 [cited 2023 Nov 7];82(6):1038–54. Available from: https://www.ncbi.nlm.nih.gov/pmc/articles/PMC8930558/
7.
Krishnamurty AT, Shyer JA, Thai M, Gandham V, Buechler MB, Yang YA, et al. LRRC15+ myofibroblasts dictate the stromal setpoint to suppress tumour immunity. Nature [Internet]. 2022 Sep 28 [cited 2024 Jun 26];611(7934):148–54. Available from: https://www.ncbi.nlm.nih.gov/pmc/articles/PMC9630141/pdf/41586_2022_Article_5272.pdf
8.
LRRC15 leucine rich repeat containing 15 [Homo sapiens (human)] - Gene - NCBI [Internet]. Nih.gov. 2025 [cited 2025 Aug 31]. Available from: https://www.ncbi.nlm.nih.gov/gene?Db=gene&Cmd=DetailsSearch&Term=131578
9.
Plikus MV, Wang X, Sinha S, Forte E, Thompson SM, Herzog EL, et al. Fibroblasts: Origins, definitions, and functions in health and disease. Cell. 2021 Jul 22;184(15):3852–72.
10.
Kawai K, Tsuno NH, Matsuhashi M, Kitayama J, Osada T, Yamada J, et al. CD11b-mediated migratory property of peripheral blood B cells. Journal of Allergy and Clinical Immunology [Internet]. 2005 Jul 1 [cited 2023 Apr 7];116(1):192–7. Available from: https://www.sciencedirect.com/science/article/pii/S0091674905005932?via%3Dihub
11.
Bruni S, Mercogliano MF, Mauro FL, R Inés, Schillaci R. Cancer immune exclusion: breaking the barricade for a successful immunotherapy. Front Oncol [Internet]. 2023 May 22 [cited 2024 May 14];13:10239871. Available from: https://www.ncbi.nlm.nih.gov/pmc/articles/PMC10239871/
12.
Mir MA. Introduction to costimulation and costimulatory molecules. In: Developing Costimulatory Molecules for Immunotherapy of Diseases. New York (NY): Springer; 2015. p. 1–43.
13.
Nielsen SR, Schmid MC. Macrophages as Key Drivers of Cancer Progression and Metastasis. Mediators of Inflammation. 2017;2017:1–11.
14.
Li K, Shi H, Zhang B, Ou X, Ma Q, Chen Y, et al. Myeloid-derived suppressor cells as immunosuppressive regulators and therapeutic targets in cancer. Signal Transduction and Targeted Therapy. 2021 Oct 7;6(1).
15.
Haist M, Stege H, Grabbe S, Bros M. The Functional Crosstalk between Myeloid-Derived Suppressor Cells and Regulatory T Cells within the Immunosuppressive Tumor Microenvironment. Cancers [Internet]. 2021 Jan 8;13(2):210. Available from: https://www.ncbi.nlm.nih.gov/pmc/articles/PMC7827203/
16.
Donges N. Random forest: a complete guide for machine learning [Internet]. Built In; 2021 [cited 2025 Aug 31]. Available from: https://builtin.com/data-science/random-forest-algorithm
17.
Alberts B, Johnson A, Lewis J, Raff M, Roberts K, Walter P. The extracellular matrix of animals. In: Molecular Biology of the Cell. 4th ed. New York (NY): Garland Science; 2002. Available from: https://www.ncbi.nlm.nih.gov/books/NBK26810/
18.
National Cancer Institute. Angiogenesis Inhibitors [Internet]. National Cancer Institute. Cancer.gov; 2018. Available from: https://www.cancer.gov/about-cancer/treatment/types/immunotherapy/angiogenesis-inhibitors-fact-sheet
19.
Zhai Y, Liang X, Deng M. Myeloid cells meet CD8+ T cell exhaustion in cancer: What, why and how. Chinese Journal of Cancer Research [Internet]. 2024 Jan 1 [cited 2025 Aug 31];36(6):616–51. Available from: https://pmc.ncbi.nlm.nih.gov/articles/PMC11724180/
20.
Jessen C, Kreß JKC, Baluapuri A, Hufnagel A, Schmitz W, Kneitz S, et al. The transcription factor NRF2 enhances melanoma malignancy by blocking differentiation and inducing COX2 expression. Oncogene. 2020 Sep 25;39(44):6841–55.
21.
Mendoza EN, Ciriolo MR, Ciccarone F. Hypoxia-Induced Reactive Oxygen Species: Their Role in Cancer Resistance and Emerging Therapies to Overcome It. Antioxidants [Internet]. 2025 Jan 15 [cited 2025 Feb 21];14(1):94–4. Available from: https://www.mdpi.com/2076-3921/14/1/94
22.
Laitala A, Erler JT. Hypoxic Signalling in Tumour Stroma. Frontiers in Oncology. 2018 May 29;8., https://www.frontiersin.org/journals/oncology/articles/10.3389/fonc.2018.00189/full
23.
Ke X, Chen C, Song Y, Cai Q, Li J, Tang Y, Han X, Qu W, Chen A, Wang H, Xu G, Liu D. Hypoxia modifies the polarization of macrophages and their inflammatory microenvironment, and inhibits malignant behavior in cancer cells. Oncol Lett. 2019 Dec;18(6):5871-5878. doi: 10.3892/ol.2019.10956.

Epub 2019 Oct 3. PMID: 31788060; PMCID: PMC6865149.
24.
Rőszer T. Understanding the Mysterious M2 Macrophage through Activation Markers and Effector Mechanisms. Mediators Inflamm. 2015;2015:816460. doi: 10.1155/2015/816460. Epub 2015 May 18. PMID: 26089604; PMCID: PMC4452191.
25.
Novak MT, Bryers JD, Reichert WM. Biomimetic strategies based on viruses and bacteria for the development of immune evasive biomaterials. Biomaterials. 2009 Mar;30(11):1989–2005. doi: 10.1016/j.biomaterials.2008.11.025.
26.
Kwa MQ, Herum KM, Brakebusch C. Cancer-associated fibroblasts: how do they contribute to metastasis? Clin Exp Metastasis. 2019 Apr;36(2):71-86. doi: 10.1007/s10585-019-09959-0. Epub 2019 Mar 7. PMID: 30847799.
27.
Chan MK, Chan EL, Ji ZZ, Chan AS, Li C, Leung KT, To KF, Tang PM. Transforming growth factor-β signaling: from tumor microenvironment to anticancer therapy. Explor Target Antitumor Ther. 2023;4(2):316-343. doi: 10.37349/etat.2023.00137. Epub 2023 Apr 28. PMID: 37205317; PMCID: PMC10185444.
28.
Frisch SM, Screaton RA. Anoikis mechanisms. Curr Opin Cell Biol. 2001 Oct;13(5):555-62. doi: 10.1016/s0955-0674(00)00251-9. PMID: 11544023.
29.
Taefehshokr N, Baradaran B, Baghbanzadeh A, Taefehshokr S, Promising approaches in cancer immunotherapy, Immunobiology, Volume 225, Issue 2, 2020, 151875, ISSN 0171-2985, https://doi.org/10.1016/j.imbio.2019.11.010.
30.
Basu K, Sinha R, Ong A, Basu T. Artificial Intelligence: How is It Changing Medical Sciences and Its Future? Indian J Dermatol. 2020 Sep-Oct;65(5):365-370. doi: 10.4103/ijd.IJD_421_20. PMID: 33165420; PMCID: PMC7640807.
31.
Beury, D. W., Carter, K. A., Nelson, C., Sinha, P., Hanson, E., Nyandjo, M., Fitzgerald, P. J., Majeed, A., Wali, N., & Ostrand-Rosenberg, S. 2016. Myeloid-Derived Suppressor Cell Survival and Function Are Regulated by the Transcription Factor Nrf2. *Journal of immunology (Baltimore, Md. : 1950)*, *196*(8), 3470–3478.
32.
Singh N, Baby D, Rajguru JP, Patil PB, Thakkannavar SS, Pujari VB. Inflammation and cancer. Ann Afr Med. 2019 Jul-Sep;18(3):121-126. doi: 10.4103/aam.aam_56_18. PMID: 31417011; PMCID: PMC6704802.
33.
Zhang F, Wang H, Wang X, Jiang G, Liu H, Zhang G, Wang H, Fang R, Bu X, Cai S, Du J. TGF-β induces M2-like macrophage polarization via SNAIL-mediated suppression of a pro-inflammatory phenotype. Oncotarget. 2016 Aug 9;7(32):52294-52306. doi: 10.18632/oncotarget.10561. PMID: 27418133; PMCID: PMC5239552.
34.
Kovaleva OV, Rashidova MA, Sinyov VV, Malashenko OS, Gratchev A. M1 macrophages - unexpected contribution to tumor progression. Front Immunol. 2025 Jul 31;16:1638102. doi: 10.3389/fimmu.2025.1638102. PMID: 40821768; PMCID: PMC12350380.
35.
Fang L., Li Y., Wang S. *et al.* TGF-β1 induces VEGF expression in human granulosa-lutein cells: a potential mechanism for the pathogenesis of ovarian hyperstimulation syndrome. *Exp Mol Med* **52**, 450–460. 2020. https://doi.org/10.1038/s12276-020-0396-y
36.
von Sengbusch A, Gassmann P, Fisch KM, Enns A, Nicolson GL, Haier J. Focal adhesion kinase regulates metastatic adhesion of carcinoma cells within liver sinusoids. Am J Pathol. 2005 Feb;166(2):585-96. doi: 10.1016/S0002-9440(10)62280-8. PMID: 15681841; PMCID: PMC1602334.
37.
Duxbury MS, Ito H, Zinner MJ, Ashley SW, Whang EE. Focal adhesion kinase gene silencing promotes anoikis and suppresses metastasis of human pancreatic adenocarcinoma cells. Surgery. 2004 May;135(5):555-62. doi: 10.1016/j.surg.2003.10.017. PMID: 15118593.
38.
Grimes DR, Jansen M, Macauley RJ, Scott JG, Basanta D. Evidence for hypoxia increasing the tempo of evolution in glioblastoma. Br J Cancer. 2020 Nov;123(10):1562-1569. doi: 10.1038/s41416-020-1021-5. Epub 2020 Aug 27. PMID: 32848201; PMCID: PMC7653934.
39.
Basak U, Sarkar T, Mukherjee S, Chakraborty S, Dutta A, Dutta S, Nayak D, Kaushik S, Das T, Sa G. Tumor-associated macrophages: an effective player of the tumor microenvironment. Front Immunol. 2023 Nov 16;14:1295257. doi: 10.3389/fimmu.2023.1295257. PMID: 38035101; PMCID: PMC10687432.
40.
DiPersio CM, Van De Water L. Integrin Regulation of CAF Differentiation and Function. Cancers (Basel). 2019 May 24;11(5):715. doi: 10.3390/cancers11050715. PMID: 31137641; PMCID: PMC6563118.
41.
Thermo Fisher Scientific. Immunolabeling [Internet]. In: Molecular Probes School of Fluorescence: Labeling your samples. Waltham (MA): Thermo Fisher Scientific; [cited 2025 Sep 1]. Available from: https://www.thermofisher.com/uk/en/home/life-science/cell-analysis/cell-analysis-learning-center/molecular-probes-school-of-fluorescence/imaging-basics/labeling-your-samples/immunolabeling.html
42.
Frantz C, Stewart KM, Weaver VM. The extracellular matrix at a glance. J Cell Sci. 2010 Dec 15;123(Pt 24):4195-200. doi: 10.1242/jcs.023820. PMID: 21123617; PMCID: PMC2995612.
43.
Belhabib I, Zaghdoudi S, Lac C, Bousquet C, Jean C. Extracellular Matrices and Cancer-Associated Fibroblasts: Targets for Cancer Diagnosis and Therapy? Cancers (Basel). 2021 Jul 11;13(14):3466.

doi: 10.3390/cancers13143466. PMID: 34298680; PMCID: PMC8303391.
44.
Storey CM, Cheng M, Altai M, Park JE, Tran J, Lueong SS, Thorek D, Mao L, Zedan W, Yuen C, Ridley A, Trajovic-Arsic M, Herrmann K, Subuhdi SK, Siddiqui BA, Lückerath K, Siveke J, Damoiseaux R, Yang X, Ulmert D. Key Regulatory Elements of the TGFβ-LRRC15 Axis Predict Disease Progression and Immunotherapy Resistance Across Cancer Types. bioRxiv [Preprint]. 2024 Nov 25:2024.11.22.624939. doi: 10.1101/2024.11.22.624939. PMID: 39651139; PMCID: PMC11623513.
45.
Purcell JW, Tanlimco SG, Hickson J, Fox M, Sho M, Durkin L, Uziel T, Powers R, Foster K, McGonigal T, Kumar S, Samayoa J, Zhang D, Palma JP, Mishra S, Hollenbaugh D, Gish K, Morgan-Lappe SE, Hsi ED, Chao DT. LRRC15 Is a Novel Mesenchymal Protein and Stromal Target for Antibody-Drug Conjugates. Cancer Res. 2018 Jul 15;78(14):4059-4072. doi: 10.1158/0008-5472.CAN-18-0327. Epub 2018 May 15. PMID: 29764866.
46.
Luo F, Mei Y, Li Y, Yang J, Xi S, Cao E, Shen C, Zhou D, Wang P, Zhou D, Cai H, CAF-derived LRRC15 orchestrates macrophage polarization and limits PD-1 immunotherapy efficacy in glioblastoma, *Neuro-Oncology*, 2025;, noaf157, https://doi.org/10.1093/neuonc/noaf157
47.
Cialdai F, Risaliti C, Monici M. Role of fibroblasts in wound healing and tissue remodeling on Earth and in space. Front Bioeng Biotechnol. 2022 Oct 4;10:958381. doi: 10.3389/fbioe.2022.958381. PMID: 36267456; PMCID: PMC9578548.
48.
Strizova Z, Benesova I, Bartolini R, Novysedlak R, Cecrdlova E, Foley LK, Striz I. M1/M2 macrophages and their overlaps - myth or reality? Clin Sci (Lond). 2023 Aug 14;137(15):1067-1093. doi: 10.1042/CS20220531. PMID: 37530555; PMCID: PMC10407193.
49.
Bruno A, Mortara L, Baci D, Noonan DM, Albini A. Myeloid Derived Suppressor Cells Interactions With Natural Killer Cells and Pro-angiogenic Activities: Roles in Tumor Progression. Front Immunol. 2019 Apr 18;10:771. doi: 10.3389/fimmu.2019.00771. PMID: 31057536; PMCID: PMC6482162.
50.
Benelli R, Zocchi MR, Poggi A. Immune Checkpoint Receptor/Ligand Expression and Chemotherapy in Colorectal Cancer. Cancers (Basel). 2023 Feb 1;15(3):914. doi: 10.3390/cancers15030914. PMID: 36765872; PMCID: PMC9913607.

Figure 1.
Kim SW, Roh J, Park CS. Immunohistochemistry for pathologists: protocols, pitfalls, and tips. J Pathol Transl Med. 2016 Dec;50(6):411–18. doi: 10.4132/jptm.2016.08.08.